to as I_g (Hille, 2001). Gating currents tend to be much smaller than the ionic currents flowing through the membrane. In order to measure gating current, the ionic current is reduced, either by replacing permeant ions with impermeant ones or by using channel blockers, though the channel blocker itself may interfere with the gating mechanism. Other methods have to be employed to eliminate leak and capacitive currents. Figure 5.7 shows recordings by Armstrong and Bezanilla (1973) of the gating current and the sodium ionic current in response to a voltage step. The gating current is outward since the positively charged residues on the membrane protein are moving outwards. It also peaks before the ionic current peaks.

Gating currents are a useful tool for the development of kinetic models of channel activation. The measurement of gating current confirmed the idea of charged gating particles predicted by the HH model. However, gating current measurements in squid giant axon have shown that the HH model is not correct at the finer level of detail (Section 5.5.3).

5.4 Modelling ensembles of voltage-gated ion channels

5.4.1 Gating particle models

Before the detailed structure and function of ion channels outlined in Section 5.1 was known, electrophysiological experiments indicated the existence of different types of channel. Various blocking and subtraction protocols led to the isolation of specific currents which displayed particular characteristics.

The A-type current

To take one example, the potassium **A-type** current, often denoted I_A, has distinct kinetics from the potassium delayed rectifier current, denoted I_{DR} or I_K or $I_{K,DR}$, originally discovered by Hodgkin and Huxley. Connor and Stevens (1971a, c) isolated the current by using ion substitution and by the differences in current flow during different voltage clamp protocols in the somata of cells of marine gastropods. The A-type current has also been characterised in mammalian hippocampal CA1 and CA3 pyramidal cells using TTX to block sodium channels (Figure 5.8).

In contrast to the delayed rectifier current, the A-type current is inactivating, and has a lower activation threshold. It has been modelled using independent gating particles by a number of authors (Connor and Stevens, 1971b; Connor *et al.*, 1977; Hoffman *et al.*, 1997; Poirazi *et al.*, 2003). In the model of Connor *et al.* (1977), the A-type current in the crustacean *Cancer magister* (Box 5.2) depends on three independent activating gating particles and one inactivating particle. In contrast, Connor and Stevens (1971b) found that raising the activating gating variable to the fourth power rather than the third power gave the best fit to the A-type current they recorded from the somata of marine gastropods.

The significance of the A-type current is illustrated clearly in simulations of two neurons, one containing sodium and potassium conductances

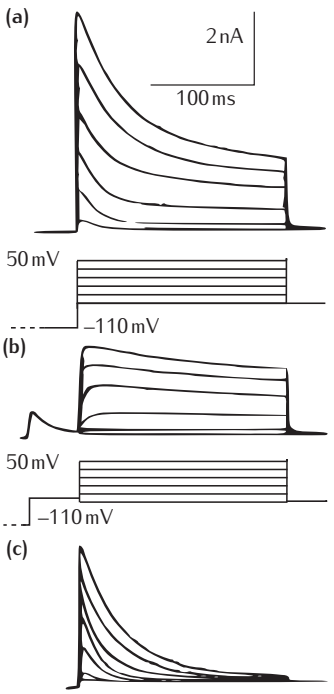

Fig. 5.8 Recordings of two types of potassium channel revealed by different voltage clamp protocols in hippocampal CA1 cells. **(a)** Family of voltage clamp current recordings from CA1 cells subjected to the voltage step protocol shown underneath. **(b)** The voltage was clamped as in **(a)**, except that there was a delay of 50 ms before the step to the depolarising voltage. **(c)** Subtraction of trace in **(b)** from trace in **(a)** reveals a transient outward current known as the A-type current. Adapted from Klee *et al.* (1995), with permission from The American Physiological Society.

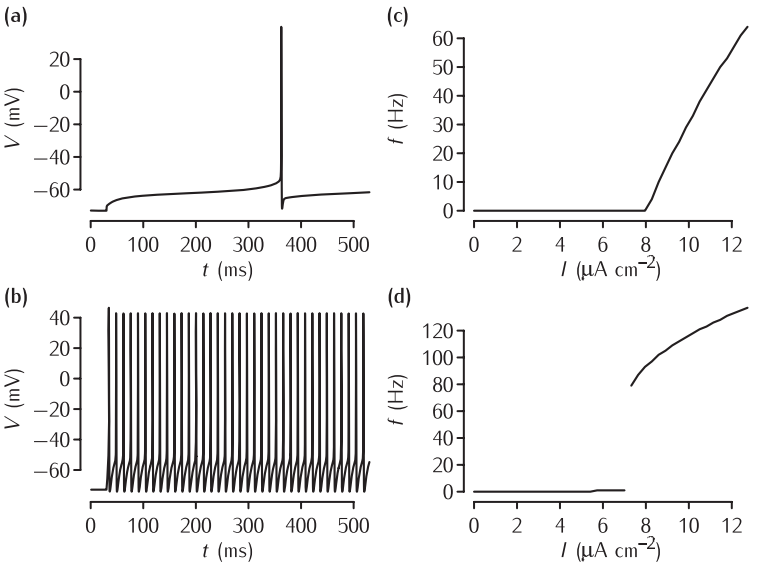

Fig. 5.9 The effect of the A-type current on neuronal firing in simulations. **(a)** The time course of the membrane potential in the model described in Box 5.2 in response to current injection of 8.21 μA cm^{-2} that is just superthreshold. The delay from the start of the current injection to the neuron firing is over 300 ms. **(b)** The response of the model to a just suprathreshold input (7.83 μA cm^{-2}) when the A-type current is removed. The spiking rate is much faster. In order to maintain a resting potential similar to the neuron with the A-type current, the leak equilibrium potential E_L is set to −72.8 mV in this simulation. **(c)** A plot of firing rate f versus input current I in the model with the A-type conductance shown in **(a)**. Note the gradual increase of the firing rate just above the threshold, the defining characteristic of Type I neurons. **(d)** The f–I plot of the neuron with no A-type conductance shown in **(b)**. Note the abrupt increase in firing rate, the defining characteristic of Type II neurons.

modelled using the Hodgkin–Huxley equations, and the other containing an A-type conductance in addition to the sodium and potassium conductances (Figure 5.9a, b). In response to sustained current injection, the model containing the A-type conductance gives rise to action potentials that are delayed compared to the action potentials in the pure HH model. This is because the A-type potassium channel is open as the membrane potential increases towards the spiking threshold, slowing the rise of the membrane potential. However, eventually the A-type current inactivates, reducing the pull on the membrane potential towards the potassium equilibrium potential and allowing the cell to fire.

Another important difference caused by the insertion of the A-type channels is apparent from plots of firing frequency versus sustained current injection (Figure 5.9c, d). Both types of model exhibit a threshold level of current below which the neuron is quiescent. In the model with the A-type conductance, the firing frequency just above the threshold is very close to zero and increases gradually. By contrast, in the HH model, as soon as the threshold is crossed, the model starts firing at a non-zero frequency. Hodgkin (1948) had noticed the two different types of f–I curve in axons from the crustacean *Carcinus maenas*. According to his classification, neurons which produce the continuous curve (Figure 5.9c) are **Type I** neurons and those which produce the curve with the abrupt change at threshold (Figure 5.9d) are **Type II** neurons. In Chapter 8 reduced models of neurons will be introduced to gain understanding of the features of the models that give rise to Type I and Type II firing patterns.

5.4.2 Thermodynamic models

In Box 5.2 there are effectively five different forms of function to fit the dependence on voltage of the rate coefficients $\alpha_m(V)$, $\beta_m(V)$ and so on: three for the Hodgkin–Huxley sodium and potassium channels (Figure 5.10), and two for the A-type potassium channel. All these forms satisfy the critical requirement of fitting the data well. However, it is desirable to base the form

Box 5.2 Model of potassium A-type current

In their model of the conductances in axons from the crab *Cancer magister*, Connor *et al.* (1977) added an A-type potassium conductance g_A with an associated equilibrium potential E_A to a current equation which includes modified versions of the Hodgkin–Huxley sodium and potassium delayed rectifier conductances:

$$C_m \frac{dV}{dt} = -g_{Na}(V - E_{Na}) - g_K(V - E_K) - g_A(V - E_A) - g_L(V - E_L).$$

The A-type conductance was derived from the experiments of Connor *et al.* (1977) at 18 °C and was modelled using independent gating particles: three activating particles a and an inactivating particle b. The kinetic equations (Section 3.2.1) written in terms of the steady state activation curves $a_\infty(V)$ and $b_\infty(V)$ and the relaxation time constants $\tau_a(V)$ and $\tau_b(V)$ are:

$$I_A = g_A(V - E_A), \qquad g_A = \overline{g}_A a^3 b,$$

$$a_\infty = \left(\frac{0.0761 \exp\left(\frac{V+99.22}{31.84}\right)}{1 + \exp\left(\frac{V+6.17}{28.93}\right)} \right)^{\frac{1}{3}}, \qquad \tau_a = 0.3632 + \frac{1.158}{1 + \exp\left(\frac{V+60.96}{20.12}\right)},$$

$$b_\infty = \frac{1}{\left(1 + \exp\left(\frac{V+58.3}{14.54}\right)\right)^4}, \qquad \tau_b = 1.24 + \frac{2.678}{1 + \exp\left(\frac{V-55}{16.027}\right)}.$$

The Hodgkin–Huxley sodium and potassium delayed rectifier conductances are modified by shifting the steady state equilibrium curves of m, h and n, multiplying the rate coefficients by a Q_{10}-derived factor of 3.8 to adjust the temperature from 6.3 °C to 18 °C, and slowing down the n variable by a factor of 2:

$$g_{Na} = \overline{g}_{Na} m^3 h, \qquad g_K = \overline{g}_K n^4,$$

$$\alpha_m = 3.8 \frac{-0.1(V + 34.7)}{\exp(-(V + 34.7)/10) - 1}, \qquad \beta_m = 3.8 \times 4 \exp(-(V + 59.7)/18),$$

$$\alpha_h = 3.8 \times 0.07 \exp(-(V + 53)/20), \qquad \beta_h = 3.8 \frac{1}{\exp(-(V + 23)/10) + 1},$$

$$\alpha_n = \frac{3.8}{2} \frac{-0.01(V + 50.7)}{\exp(-(V + 50.7)/10) - 1}, \qquad \beta_n = \frac{3.8}{2} 0.125 \exp(-(V + 60.7)/80).$$

The remaining parameters of the model are:

$$C_m = 1\,\mu\text{F cm}^{-2} \quad E_{Na} = 50\,\text{mV} \quad \overline{g}_{Na} = 120.0\,\text{mS cm}^{-2}$$
$$E_K = -77\,\text{mV} \quad \overline{g}_K = 20.0\,\text{mS cm}^{-2}$$
$$E_A = -80\,\text{mV} \quad \overline{g}_A = 47.7\,\text{mS cm}^{-2}$$
$$E_L = -22\,\text{mV} \quad g_L = 0.3\,\text{mS cm}^{-2}$$

In all the equations described here, the voltage is 5 mV lower than the values of Connor *et al.* (1977), to match the parameters used in Chapter 3.

This approach of adapting a model from a different organism contrasts with that taken in the earlier model of *Anisodoris* (Connor and Stevens, 1971b), where many of the values for the steady state variables are piecewise linear fits to recorded data. The two models give similar results.

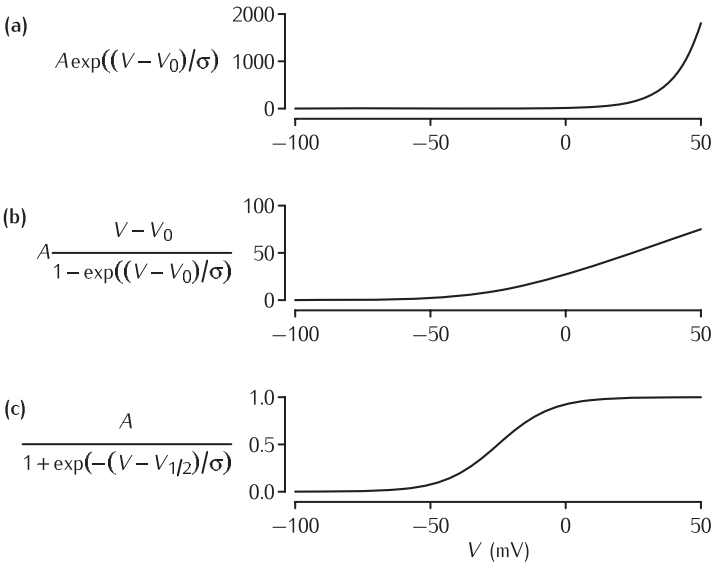

Fig. 5.10 In the HH model (Box 3.5), the voltage-dependent rate coefficients are described by three different types of equation. **(a)** The rate coefficients β_m, α_h and β_n are described by exponential functions of the voltage V. A, V_0 and σ are constants. This fits the empirical rate coefficients α_m and α_n at low membrane potentials, but overestimates the rates at higher membrane potentials. **(b)** Linear-exponential functions produce lower rate coefficients at higher voltages and fit the data well. However, it gives rate coefficients that are too high for the gating variable h at high voltages, where β_h saturates. **(c)** β_h can be described by a rate coefficient with a sigmoidal function where $V_{1/2}$ is the half activation voltage and where σ is the inverse slope.

The sigmoid curve is similar to Hodgkin and Huxley's fit to n_∞ (Figure 3.10) using the functions for α_n and β_n from Equation 3.13.

of these functions as much as possible on the biophysical theory of channels, since fitting to the most principled function is likely to minimise errors due to fitting.

In thermodynamic models (Borg-Graham, 1989; Destexhe and Huguenard, 2000), the rate coefficients are given by functions derived from the **transition state theory** (or energy barrier model) of chemical reactions, to be discussed in Section 5.8. For a gating particle represented by a gating variable x, the steady state activation is given by a sigmoid curve:

$$x_\infty = \frac{1}{1+\exp(-(V-V_{1/2})/\sigma)}, \tag{5.1}$$

where $V_{1/2}$ is the half-activation voltage and σ is the inverse slope, as shown in Figure 5.11. The corresponding time constant is:

$$\tau_x = \frac{1}{\alpha'(V)+\beta'(V)} + \tau_0, \tag{5.2}$$

where τ_0 is a rate-limiting factor and the expressions for α'_x and β'_x are exponentials that depend on $V_{1/2}$ and σ, a maximum rate parameter K and a parameter δ, which controls the skew of the τ curve:

$$\begin{aligned} \alpha'_x(V) &= K\exp\left(\frac{\delta(V-V_{1/2})}{\sigma}\right) \\ \beta'_x(V) &= K\exp\left(\frac{-(1-\delta)(V-V_{1/2})}{\sigma}\right). \end{aligned} \tag{5.3}$$

Figure 5.11 shows plots of the time constant as a function of voltage.

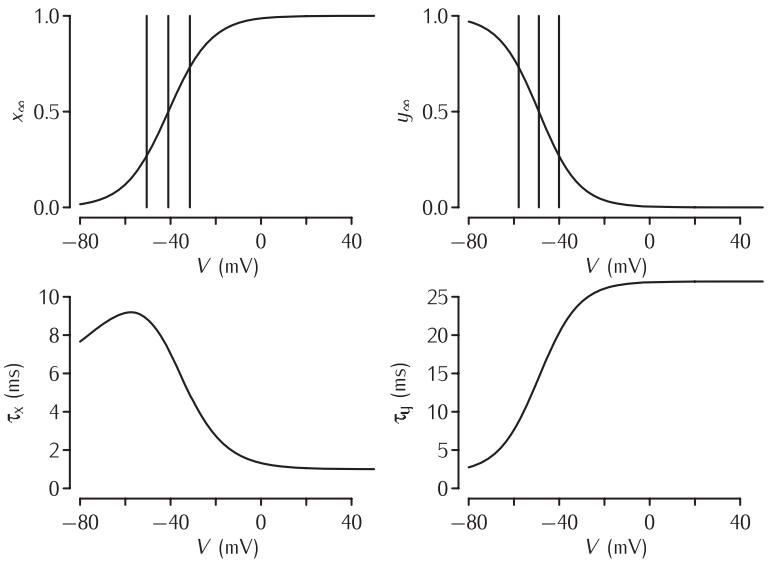

Fig. 5.11 Plots of the steady states x_∞ and y_∞ of the activation and inactivation and of the corresponding time constants τ_x and τ_y of a thermodynamic model of the A-type current due to Borg-Graham (1999). The curves for the steady states and time constants are derived from Equations 5.1 and 5.2, respectively. In the steady state curves, the middle vertical line indicates the half-activation voltage, $V_{1/2}$, and the two flanking lines indicate $V_{1/2} - \sigma$ and $V_{1/2} + \sigma$. The parameters for the activation (x) curves are $V_{1/2} = -41$ mV, $\sigma = 9.54$ mV, $K = 8 \times 10^2$ ms^{-1}, $\delta = 0.85$, $\tau_0 = 1$ ms. The parameters for the inactivation (y) curves are $V_{1/2} = -49$ mV, $\sigma = -8.90$ mV, $K = 4 \times 10^2$ ms^{-1}, $\delta = 1$, $\tau_0 = 2$ ms. The sign of σ determines whether the curve has a positive or negative slope.

The term τ_0 is in fact an addition to the basic transition state theory account. However, if it is set to zero, the effective time constant $\tau_x = \alpha_x/(\alpha_x + \beta_x)$ can go to zero. In practice, transitions tend not to happen this quickly (Patlak, 1991), and it is evident from the equations for τ_x that the rate-limiting factor τ_0 leads to a minimum time constant.

The steady state value x_∞ and time constant τ_x can be converted into equations for the rate coefficients α_x and β_x (Equation 3.10), giving:

$$\alpha_x(V) = \frac{\alpha'_x(V)}{\tau_0(\alpha'_x(V) + \beta'_x(V)) + 1}$$
$$\beta_x(V) = \frac{\beta'_x(V)}{\tau_0(\alpha'_x(V) + \beta'_x(V)) + 1}. \quad (5.4)$$

Calcium channels

Similar principles apply to modelling calcium channels, such as the T- and L-types, voltage clamp recordings of which are shown in Figure 5.6. The only difference is that because of the inward rectifying nature of the I–V relationship for calcium due to low intracellular concentration of calcium, the GHK current equation (Box 2.4) is often used in modelling calcium channels. For the non-inactivating L-type channel, the permeability can be modelled with two activating particles m, and the inactivating T-type channel can be modelled with two activating particles m and one inactivating particle h (Borg-Graham, 1999). In both cases $1/K$ is small compared to τ_0, so the time constants τ_m and τ_h are effectively independent of voltage. Table 5.2 shows typical values of $V_{1/2}$, σ and τ_0 for these channels. There is evidence that the L-type channels require calcium to inactivate. This could be modelled using an extra calcium-dependent inactivation variable (Section 5.6).

Other types of voltage-gated channels

There are many more types of current, some of which are listed in Table 5.2. They can be characterised broadly according to whether they are activated by voltage or calcium or both, in the case of I_C, and whether they display fast or slow activation and inactivation.

The half activation voltage and the slope of these curves varies between currents. The values of these quantities listed in Table 5.2 are only indicative as there can be substantial variations between different preparations; for example, variations in temperature (Section 3.4), expression of auxiliary subunits (Section 5.1), or which modulators are present inside and outside the cell. Table 5.2 also lists the principal channel proteins which are proposed to underlie each type of current. In some cases, the same protein appears to be responsible for different currents; for example, $Na_v1.1$ appears to underlie I_{Na} and the persistent sodium current I_{NaP}. This may be possible because of the differences in auxiliary subunit expression.

5.5 Markov models of ion channels

In the channel models covered so far, the gating variables, such as n, m and h in the HH model, represent the probability of one of a number of gating particles being in an open position; the probability of the entire gate (or channel) being open is the product of these variables raised to a power, indicating that the gating particles act independently. This section introduces **Markov models** of ion channels in which the probability of the entire ion channel being in one of a number of possible states is represented, and one or more of these states may correspond to the ion channel being open. This allows data to be fitted more accurately, though at the expense of having a greater number of parameters to fit. Ideally, each state would correspond to one channel protein conformation, but in practice even complex Markov models are approximations of the actual dynamics of the channel.

Markov models are fundamentally probabilistic models in which the state changes are random. This makes them an appropriate framework in which to model the microscopic currents due to the opening and closing of single ion channels or ensembles of a small number of ion channels. However, when large numbers of channels are present, the recorded currents are smooth because the fluctuations of individual channels are averaged out, and it is approximately correct to interpret Markov models deterministically. In this section the deterministic interpretation of Markov models will be introduced. The techniques required for the stochastic interpretation of Markov models are introduced in Section 5.7.

The term 'kinetic scheme' is often used interchangeably with Markov model, especially when interpreting Markov models deterministically (Cannon and D'Alessandro, 2006).

5.5.1 Kinetic schemes

The states and possible transitions between them in a Markov model are represented by a **kinetic scheme**. An example of a kinetic scheme is:

$$C_1 \underset{k_{-1}}{\overset{k_1}{\rightleftharpoons}} C_2 \underset{k_{-2}}{\overset{k_2}{\rightleftharpoons}} C_3 \underset{k_{-3}}{\overset{k_3}{\rightleftharpoons}} C_4 \underset{k_{-4}}{\overset{k_4}{\rightleftharpoons}} O. \tag{5.5}$$

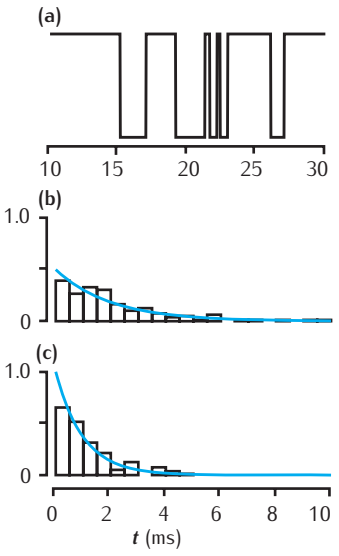

Fig. 5.15 Features of a two-state kinetic scheme. **(a)** Simulated sample of the time course of channel conductance of the kinetic scheme described in Scheme 5.13. The parameters are $\alpha = 1\,\text{ms}^{-1}$ and $\beta = 0.5\,\text{ms}^{-1}$. **(b)** Histogram of the open times in a simulation and the theoretical prediction of $0.5e^{-0.5t}$ from Equation 5.14. **(c)** Histogram of the simulated closed times and the theoretical prediction e^{-t}.

5.7 Modelling single channel data

Markov models of channels were introduced in Section 5.5, but only their deterministic interpretation was considered. In this section the underlying probabilistic basis of Markov models is outlined. This provides tools for analysing single channel data and for simulating Markov models.

5.7.1 Markov models for single channels

Markov models all obey the **Markov property**: the probability of a state transition depends only on the state the channel is in and the probabilities of transitions leading from that state, not on the previous history of transitions. This can be illustrated by considering a very simple kinetic scheme in which the channel can be in an open state (O) or a closed state (C):

$$\text{C} \underset{\beta}{\overset{\alpha}{\rightleftharpoons}} \text{O}, \tag{5.13}$$

where α and β are transition probabilities which can depend on voltage or ligand concentration, analogous to the rate coefficients in the deterministic interpretation. With the channel in the closed state, in an infinitesimally small length of time Δt it has a probability of $\alpha\Delta t$ of moving to the open state; if it is in the open state, it has a probability of $\beta\Delta t$ of moving back to the closed state. This scheme can be simulated exactly using the algorithm to be described in Section 5.7.2 to produce conductance changes such as those shown in Figure 5.15a. Each simulation run of the scheme produces a sequence of random switches between the C and O states.

A key statistic of single channels is the distribution of times for which they dwell in open or closed conductance states. Histograms of the channel open and closed times can be plotted, as shown in Figures 5.15b and 5.15c for the most basic two-state scheme (Scheme 5.13). By considering the time steps Δt to be infinitesimally small, the transition from one state to another acts as a Poisson process, in which the inter-event intervals are distributed exponentially:

$$\begin{aligned} \text{Prob(in closed state for time } t) &= \alpha \exp(-\alpha t) \\ \text{Prob(in open state for time } t) &= \beta \exp(-\beta t). \end{aligned} \tag{5.14}$$

The mean closed time is $1/\alpha$, meaning that the higher the forward reaction rate α the shorter the time during which the channel will stay in the closed state. Similarly, the mean open time is $1/\beta$.

Open and closed time histograms extracted from experimental recordings of single channel currents do not tend to have this simple exponential structure. For example, the closed time distribution of calcium channels in bovine chromaffin cells (Figure 5.16) is fitted more closely by a double exponential than by a single exponential (Fenwick *et al.*, 1982). As each exponential has a characteristic time constant, this indicates that there are at least three timescales in the system. Since each transition is associated with a time constant, this means that a kinetic scheme with at least three states is required to model the data. The data shown in Figure 5.16 can be modelled

by a three-state scheme with two closed states (C_1 and C_2) and one open state (O):

$$C_1 \underset{\beta_1}{\overset{\alpha_1}{\rightleftharpoons}} C_2 \underset{\beta_2}{\overset{\alpha_2}{\rightleftharpoons}} O. \tag{5.15}$$

In this case it is possible to determine the four transition probabilities from the time constant of the open time distribution, the fast and slow time constants of the closed time distribution and the ratio of the fast and slow components of the closed time distribution.

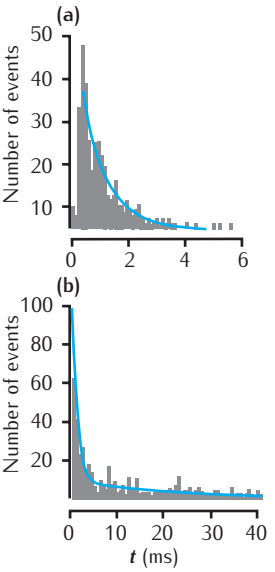

Fig. 5.16 Distributions of open and closed times of single Ca^{2+} channels from bovine chromaffin cells recorded by Fenwick *et al.* (1982). The distribution of open times is fitted by a single exponential with a time constant of 0.81 ms, but the distribution of closed times is fitted by two exponentials with time constants of 1.05 ms and 25.5 ms. Adapted from Fenwick *et al.* (1982), with permission from John Wiley & Sons Ltd.

5.7.2 Simulating a single channel

Within a single compartment of a compartmental model there is generally a population of more than one ion channel of the same type. The simulation of each ion channel can be considered individually. This is less efficient than the method of the Stochastic Simulation Algorithm (SSA) (Section 6.9). However, it makes the principle of stochastic simulation clear, so will be considered in this section.

As an example, consider the five-state potassium channel scheme (Scheme 5.5) with the rate coefficients given by the HH model. In this kinetic description, transitions between states depend only on the membrane potential. The method described in this section is efficient, but only works when the membrane potential is steady, as it is under voltage clamp conditions.

In order to simulate an individual potassium channel using this scheme, an initial state for the channel must be chosen. It is usual to select a state consistent with the system having been at rest initially. The probability that the channel is in each of the five states can then be calculated. For example, the probability of being in state C_1 given initial voltage V_0 is:

$$P_{C_1} = (1 - n_\infty(V_0))^4 = \left(1 - \frac{\alpha_n(V_0)}{\alpha_n(V_0) + \beta_n(V_0)}\right)^4. \tag{5.16}$$

C_4 is the state in which all four of the particles are closed. As described in Chapter 3, the probability of a particle being in the closed state is given by $1 - n_\infty(V_0)$. Consequently, the probability that all four of the particles are in the closed state is $(1 - n_\infty(V_0))^4$. The probability of being in state C_2, where exactly one of the four particles is in the open state with the remainder closed is:

$$P_{C_2} = \binom{4}{3}(1 - n_\infty(V_0))^3 n_\infty(V_0), \tag{5.17}$$

where $\binom{4}{3}$ is the number of possible combinations in which any three of the four particles can be in the closed state. In a similar manner, the probabilities of the particle being in states C_3, C_4 and O respectively, given the initial

$\binom{n}{k}$ is the number of combinations each of size k that can be drawn from an unordered set of n elements. This is given by:

$$\binom{n}{k} = \frac{n!}{k!(n-k)!}.$$

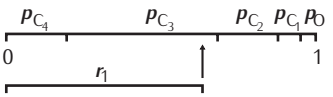

Fig. 5.17 The initial probabilities of each state of the kinetic model can be used to divide a unit line. The example uses the five-state Hodgkin and Huxley channel model given in Scheme 5.5 with initial voltage $V_0 = -60$.

voltage V_0 are given by:

$$\begin{aligned} P_{C_3} &= \binom{4}{2}(1-n_\infty(V_0))^2 n_\infty(V_0)^2 \\ P_{C_4} &= \binom{4}{1}(1-n_\infty(V_0)) n_\infty(V_0)^3 \\ P_O &= n_\infty(V_0)^4. \end{aligned} \tag{5.18}$$

The initial state for the simulation is selected stochastically by assigning to each probability a section of a line running from 0 to 1 (Figure 5.17), drawing a random number r_1 between 0 and 1 from a uniform distribution, and selecting the initial state according to where r_1 lies on the line.

The next step in the simulation is to determine how long the system resides in a state, given the membrane potential V. Suppose the channel is in state C_1. As state transitions act as a Poisson process (Section 5.7.1), the probability that the system remains in state C_1 for duration τ is given by:

$$P_{C_1}(\tau) = 4\alpha_n \exp(-4\alpha_n \tau), \tag{5.19}$$

where $4\alpha_n$ is the rate at which state C_1 makes the transition to state C_2 at voltage V (the V dependency has been omitted from α_n for clarity). By converting this distribution into a cumulative distribution, another random number r_2, between 0 and 1, can be used to calculate the duration:

$$\tau = -\frac{\ln(r_2)}{4\alpha_n}. \tag{5.20}$$

Similar probabilities for the other states can be calculated:

$$\begin{aligned} P_{C_2}(\tau) &= (3\alpha_n + \beta_n)\exp(-(3\alpha_n + \beta_n)\tau) \\ P_{C_3}(\tau) &= (2\alpha_n + 2\beta_n)\exp(-(2\alpha_n + 2\beta_n)\tau) \\ P_{C_4}(\tau) &= (\alpha_n + 3\beta_n)\exp(-(\alpha_n + 3\beta_n)\tau) \\ P_O(\tau) &= 4\beta_n \exp(-4\beta_n \tau) \end{aligned} \tag{5.21}$$

and the random duration calculated by replacing $4\alpha_n$ in Equation 5.20 with the appropriate rate.

Finally, once the system has resided in this state for the calculated duration, its next state must be chosen. In this example, in states C_1 and O there is no choice to be made, and transitions from those states can only go to one place. For the intermediate states, transition probabilities are used to select stochastically the next state. The probability of the transitions from state C_2 to C_1 or C_3 are given by:

$$\begin{aligned} P_{C_2,C_1} &= \frac{\beta_n}{\beta_n + 3\alpha_n} \\ P_{C_2,C_3} &= \frac{3\alpha_n}{\beta_n + 3\alpha_n}. \end{aligned} \tag{5.22}$$

Clearly, the sum of transition probabilities away from any state add to 1. To choose the new state stochastically, we can use the technique for selecting the initial state illustrated in Figure 5.17.

5.9 Ion channel modelling in theory and practice

This chapter has concentrated on the theory of modelling ion channels. It has been shown how ion channel models of varying levels of complexity can be used to describe voltage- and ligand-gated ion channel types. Ideally, in order to construct a realistic model of a neuron, the computational neuroscientist should follow Hodgkin and Huxley by characterising the behaviour of each type of channel in the neuron at the temperature of interest, and producing, at least, an independent gating model of the channel.

In the real world, this does not tend to happen because the effort involved is prohibitive compared to the rewards. When faced with building a model containing a dozen channel types, rather than running experiments, typically the computational neuroscientist searches the literature for data from which to construct a model. The data is not necessarily from the neuron type, brain area or even species in question, and quite probably has been recorded at a temperature that differs from the model temperature. With the advent of databases of models such as ModelDB (Appendix A.2) it is possible to search for channel models which have already been implemented in simulation code. While differing temperatures can be corrected for, it is not possible to correct for the mismatch in the preparations and species. This means that the vast majority of compartmental models are incorrect in some details. However, even compartmental models with inexact models of channels are of utility, as they give insights into the types of behaviours possible from a neuron, and they force assumptions in arguments to be made explicit.

In fact, the situation is even more complicated. Various studies have shown that the distribution of channels varies from neuron to neuron, even when the neurons are of the same type (Marder and Prinz, 2002). However, the overall behaviour of the neurons is conserved between different members of the class. For example, in a relatively simple model of the crab stomatogastric ganglion cell with five conductances, Goldman *et al.* (2001) explored the behaviour of the model with combinations of the density of three of the conductances (a calcium conductance, a calcium-dependent potassium conductance and the A-type potassium conductance). This gave a 3D grid of parameter values, and the behaviour of the cell – quiescent, tonically firing or bursting – was determined at each grid point. The simulations showed that many possible combinations of ion channel can give rise to the same behaviours. In order to preserve given behaviours, channel densities are regulated dynamically (see Turrigiano and Nelson, 2004 for review). It may be that from the point of view of understanding cellular function, it is more important to understand these regulatory mechanisms than to model ion channels at the greatest level of detail.